Journal of Computational Physics **170,** 231–260 (2001)
doi:10.1006/jcph.2001.6734, available online at http://www.idealibrary.com on IDEAL®

A Multidomain Spectral Method for Scalar and Vectorial Poisson Equations with Noncompact Sources

P. Grandclément, S. Bonazzola, E. Gourgoulhon, and J.-A. Marck

Département d'Astrophysique Relativiste et de Cosmologie (UMR 8629 du C.N.R.S.), Observatoire de Paris, Section de Meudon, F-92195 Meudon Cedex, France
E-mail: Philippe.Grandclement@obspm.fr

Received March 22, 2000; revised January 26, 2001

We present a spectral method for solving elliptic equations which arise in general relativity, namely three-dimensional scalar Poisson equations, as well as generalized vectorial Poisson equations of the type $\Delta\vec{N} + \lambda\vec{\nabla}(\vec{\nabla}\cdot\vec{N}) = \vec{S}$ with $\lambda \neq -1$. The source can extend in all the Euclidean space $\mathbf{R}^3$, provided it decays at least as r^{-3}. A multidomain approach is used, along with spherical coordinates (r, θ, ϕ). In each domain, Chebyshev polynomials (in r or $1/r$) and spherical harmonics (in θ and ϕ) expansions are used. If the source decays as r^{-k} the error of the numerical solution is shown to decrease at least as $N^{-2(k-2)}$, where N is the number of Chebyshev coefficients. The error is even evanescents; i.e., it decreases as $\exp(-N)$, if the source does not contain any spherical harmonics of index $l \geq k-3$ (scalar case) or $l \geq k-5$ (vectorial case).

Key Words: scalar and vectorial Poisson equations; spectral methods; Gibbs phenomenon; general relativity.

1. INTRODUCTION

1.1. *Scalar and Vectorial Poisson Equations with Noncompact Sources*

The most common elliptic equations which occur in numerical relativity (for a recent review see [1]) are the scalar Poisson equation

$$\Delta F = S \tag{1}$$

and the (generalized) vector Poisson equation

$$\Delta\vec{N} + \lambda\vec{\nabla}(\vec{\nabla}\cdot\vec{N}) = \vec{S}, \tag{2}$$

0021-9991/01 $35.00

where λ is a constant different from -1, typically $\lambda = 1/3$. Contrary to the Newtonian case, where the source term S contains only the matter density, the sources of these equations have a noncompact support. Moreover, the Einstein equations being nonlinear, the sources S and $\vec{S}$ depend (usually quadratically) on the solutions F and $\vec{N}$. This means that Eqs. (1) and (2) must be solved by iteration.

More precisely, within the $3+1$ formalism (also called *Cauchy formulation*) of general relativity (see [2] for a review), the 10 Einstein equations can be decomposed into a set of six second-order evolution equations and four constraint equations: a scalar one, the so-called *Hamiltonian constraint*, and a vectorial one, the so-called *momentum constraint* (see [3] for an extensive discussion of the constraints equations). The PDE type (i.e., hyperbolic, parabolic, or elliptic) of these equations depends on the coordinates chosen to describe the space–time manifold. Let us recall that within the $3+1$ formalism, the space–time is foliated in a family of space-like slices Σ_t, labeled by the time coordinate t. The space–time 4-metric is then entirely described by the induced 3-metric γ_{ij} of the hypersurfaces Σ_t along with the extrinsic curvature tensor K_{ij} of Σ_t.

In this context, a typical example of Eq. (1) is the equation for the lapse function for the choice of time coordinate corresponding to a *maximal slicing* of space–time[1] (see, e.g., [4]). Another example is provided by York treatment of the initial-value problem of general relativity [5], according to which the Hamiltonian constraint equation results in an elliptic equation of type (1) for the conformal factor of the spatial metric γ_{ij}, with a term F^{-7} in S.

Regarding the vector Poisson equation (2), it also appears in York formulation of the initial-value problem for the vector which enters in the longitudinal part of the transverse-traceless decomposition of the extrinsic curvature tensor K_{ij}. Indeed the momentum constraint determines the longitudinal part of K_{ij} according to the equation[2]

$$\nabla_j K^{ij} = 8\pi J^i, \tag{3}$$

where ∇_j is the covariant derivative associated with the 3-metric γ_{ij}, J^i is the matter momentum density, and maximal slicing is assumed ($K^i_i = 0$). More generally, the vector Poisson equation (2) with $\lambda = 1/3$ occurs each time one has to perform the transverse-traceless decomposition of a symmetric tensor field T^{ij} defined on a Riemannian three-manifold with metric γ_{ij}. Following [5, 6], this decomposition writes

$$T^{ij} = T^{ij}_{\mathrm{TT}} + (LY)^{ij} + \frac{1}{3}T\gamma^{ij}, \tag{4}$$

where $T = \gamma_{kl}T^{kl} \cdot T^{ij}_{\mathrm{TT}}$ is the transverse-traceless part, $(LY)^{ij}$ the longitudinal trace-free one, and $\frac{1}{3}T\gamma^{ij}$ the trace part. The longitudinal part is expressible in terms of a vector Y^i, by means of the conformal Killing operator:

$$(LY)^{ij} = \nabla^i Y^j + \nabla^j Y^i - \frac{2}{3}\gamma^{ij}\nabla_k Y^k. \tag{5}$$

Performing the decomposition reduces to the finding of the vector field $\vec{Y}$. Considering the

[1] This Poisson equation for the lapse function reduces to the usual Poisson equation for the gravitational potential at the Newtonian limit.

[2] Einstein convention of summation on repeated indices is used.

divergence of Eq. (4), $\vec{Y}$ appears to be the solution of the equation

$$\Delta Y^i + \frac{1}{3}\nabla^i(\nabla_j Y^j) = \nabla_j\left(T^{ij} - \frac{1}{3}T\gamma^{ij}\right) - R^i_j Y^j, \tag{6}$$

where R^i_j is the Ricci tensor associated with the metric γ_{ij}. This is a vectorial Poisson equation of type (2) with $\lambda = \frac{1}{3}$ (involving the so-called conformal Laplace operator). Let us mention that, in the general case, it must be solved by iteration for $\vec{Y}$ is present in the source term.

Another example of the vectorial Poisson equation (2) is provided by the so-called *minimal distortion* [4] choice of coordinates in the spatial hypersurfaces Σ_t. The unknown vector $\vec{N}$ is in this case the *shift vector* which defines the propagation of the spatial coordinates x^i from one slice Σ_t to the next one Σ_{t+dt}. It is this vectorial Poisson equation, which is a special form of Eq. (2) with $\lambda = \frac{1}{3}$, that originally motivated our study of this subject. Let us mention that the conformal Killing operator and the associated vectorial Poisson equation also appear in the "thin-sandwich" formulation, where the spatial geometry is given on two close hypersurfaces (see [3, 7] for more details).

1.2. *Treatment by Means of Spectral Methods*

Solving elliptic equations is often considered as a CPU time consuming task. Spectral methods [8, 9] seems attractive in this respect because they provide accurate results with reasonable sampling, as compared with finite difference methods, for example. We refer the interested reader to [10, 11] for a review of the use of spectral methods in relativistic astrophysics. Let us simply mention here that our group has previously developed a spectral method, using Chebyshev polynomials and spherical harmonics to solve three-dimensional scalar Poisson equations with a compact source [12]. However, as recalled above, the elliptic equations which arise from numerical relativity have noncompact sources. This means in particular that infinity is the only location to impose exact boundary conditions (flat space–time). In order to tackle this, we have introduced a multidomain approach [13] within which the last domain extends up to infinity, thanks to some compactification. This approach has another nice feature, for it is avoiding Gibbs phenomena: a physical discontinuity can be located at the boundary between two domains so that all the considered fields are smooth in each domain.

In this article, we extend the single-domain spectral method for the scalar Poisson equation (1) presented in [12] to the multidomain case, which enables in particular to treat noncompact sources provided they decay at least as r^{-3} when $r \to \infty$. Based on this scalar Poisson solver, we treat the generalized vectorial Poisson equation (2). We consider three different schemes proposed in the literature to reduce the resolution of (2) to four scalar Poisson equations, namely the schemes of Bowen and York [14], Oohara and Nakamura [15], and Oohara, Nakamura, and Shibata [16]. These schemes have been originally implemented on finite (single) domains and with finite difference methods. We study here their applicability to infinite domains and spectral methods.

The solvers presented in this work deal with three-dimensional flat spaces where $\vec{\nabla}$ denotes the ordinary derivation. More general cases (i.e., Laplacian operator associated with a curved metric) can be solved by iteration. In all the following we will assume that there exists a unique solution of both the scalar and the vectorial equation that is $\mathcal{C}^\infty$ by parts,

$\mathcal{C}^1$ everywhere, and that is going to zero at infinity. For known results about the existence and uniqueness of solution of partial derivative systems see, for example, [17].

This paper is organized as follows. In Section 2 we present the numerical scheme used to solve the scalar Poisson equation with our multidomain spectral method. This scheme is tested in Section 3 using comparison with analytical solutions of various behaviors. This study leads us to establish the convergence properties of the algorithm. Section 4 is devoted to the study the three different schemes mentioned above to solve the vectorial Poisson equation (2). As for the scalar Poisson equation, the implemented schemes are tested in Section 5 and their convergence properties exhibited. In Section 6 we give some indication about some extensions of this work that have been successfully conducted or under investigation.

2. SCALAR POISSON EQUATION

2.1. *Spectral Expansions*

As described in previous articles [10, 12], spherical coordinates (r, θ, ϕ) are used; the fields are expanded in spherical harmonics $Y_l^m(\theta, \phi)$ and a Chebyshev expansion is performed with respect to the r coordinate. Doing so the resolution of the scalar Poisson equation is reduced to find, for each couple (l, m) the solution of

$$\frac{\mathrm{d}^2 f}{\mathrm{d}r^2} + \frac{2}{r}\frac{\mathrm{d}f}{\mathrm{d}r} - \frac{l(l+1)}{r^2} f = s(r), \tag{7}$$

where f and s are functions of r solely, being respectively the coefficients of Y_l^m in the solution F and in the source S.

f and s are expanded in Chebyshev polynomials (hereafter referred to as T_i for the polynomial of order i) so that the inversion of the operator on the left-hand side of Eq. (7) is reduced to a matrix inversion.

As recalled above, the present work improves that presented in [12] for we are allowing a source that is not compactly supported. To take care of this, we will divide space in three type of domains, following [13]

- One *kernel*, a sphere centered at the origin and being the only domain considered in [12]. In such a domain r is given by $r = \alpha x$, where $x \in [0, 1]$, with $\alpha > 0$. The functions are expanded in Chebyshev polynomials in x with a definite parity to ensure regularity at the origin: only even (resp. odd) polynomials are involved for l even (resp. odd).
- An arbitrary number, including zero, of *shells*, domains where $r = \alpha x + \beta$, $x \in [-1, 1]$. We have the following conditions : $\alpha > 0$ and $\beta \geq \alpha$, so that r is increasing with x and never equal to zero. In the shells, the functions are expanded in usual Chebyshev polynomials, with no parity requirement.
- One external domain, extending to infinity, where r is given by $u = r^{-1} = \alpha(x - 1)$, α being negative, and $x \in [-1, 1]$. Once more the functions are given as a sum of Chebyshev polynomial in x.

2.2. *The Matrices*

Before doing any operator inversion, one has to take care of singularities at the origin and at infinity. For example, because of division by r^2, the solution of the equation, must be decreasing as r^2 at the origin to be associated with a nonsingular source. We choose to treat that by subtracting finite parts of the solution at the point of singularity.

Before describing that more precisely, let us mention another method for solving that problem, presented in [12]. In [12] the functions are expanded on a new set of basis functions that verify individually the regularity conditions (Galerkin basis). For example, $T_{i+2} + T_i$ is used in the kernel, making all the basis functions decrease as r^2 at the origin.

• In the kernel, we have to take care of a singularity at the origin due to the division by r^2. To avoid this we construct an operator without the finite part of f at $x = 0$. Thus the operator is, expressed in terms of x,

$$Af = \frac{\mathrm{d}^2 f}{\mathrm{d}x^2} + \frac{2}{x}\left(\frac{\mathrm{d}f}{\mathrm{d}x} - \frac{\mathrm{d}f}{\mathrm{d}x}(0)\right) - \frac{l(l+1)}{x^2}\left(f - f(0) - x\frac{\mathrm{d}f}{\mathrm{d}x}(0)\right), \tag{8}$$

the source s being multiplied by α^2.

• In the shells there is no singularity, so we can multiply the source by $\frac{r^2}{\alpha^2}$ and invert the following operator

$$Af = \left(x + \frac{\beta}{\alpha}\right)^2 \frac{\mathrm{d}^2 f}{\mathrm{d}x^2} + 2\left(x + \frac{\beta}{\alpha}\right)\frac{\mathrm{d}f}{\mathrm{d}x} - l(l+1)f. \tag{9}$$

• In the external domain Eq. (7), once rewritten in terms of $u = \frac{1}{r}$, becomes

$$u^4\left(\frac{\mathrm{d}^2 f}{\mathrm{d}u^2} - \frac{l(l+1)}{u^2}f\right) = s. \tag{10}$$

We consider the three following possibilities.

—First multiplying the source by r^4 in the external domain, a singularity occurs at $r = \infty$; that is, $x = 1$. We handle it like in the kernel, by subtraction of the finite part of f in 1, and we use the following operator

$$Af = \frac{\mathrm{d}^2 f}{\mathrm{d}x^2} - \frac{l(l+1)}{(x-1)^2}\left(f - f(1) - (x-1)\frac{\mathrm{d}f}{\mathrm{d}x}(1)\right). \tag{11}$$

—If the source is multiplied by r^3, a singularity occurs $r = \infty$; that is, $x = 1$ and is handled by the finite part method, so that the operator becomes

$$Af = (x-1)\frac{\mathrm{d}^2 f}{\mathrm{d}x^2} - \frac{l(l+1)}{(x-1)}(f - f(1)). \tag{12}$$

—If the source is only multiplied by r^2, we invert the nonsingular operator

$$Af = (x-1)^2\frac{\mathrm{d}^2 f}{\mathrm{d}x^2} - l(l+1)f. \tag{13}$$

In all cases we have to multiply s by α^2. Let us stress that those three operators are not fully equivalent in actual physical calculations based on iterative schemes. The effective source (i.e., $r^k S$) being given, the solution will have less high-frequency terms (Chebyshev polynomials of high-order), if the number k is high. Those high-frequency terms may cause instabilities in an iterative procedure, so we always use the r^4S scheme except for a source decreasing like r^3S at infinity.

As an illustration, here is the matrix constructed in the kernel, with $l = 2$ and nine coefficients in r (Chebyshev polynomials $T_0, T_2, \ldots, T_{16}$)

$$\begin{pmatrix} 0 & 0 & 56 & 96 & 304 & 480 & 936 & 1344 & 2144 \\ 0 & 0 & 56 & 240 & 472 & 1056 & 1656 & 2832 & 3992 \\ 0 & 0 & 0 & 144 & 432 & 848 & 1632 & 2512 & 3984 \\ 0 & 0 & 0 & 0 & 264 & 688 & 1320 & 2336 & 3528 \\ 0 & 0 & 0 & 0 & 0 & 416 & 1008 & 1888 & 3168 \\ 0 & 0 & 0 & 0 & 0 & 0 & 600 & 1392 & 2552 \\ 0 & 0 & 0 & 0 & 0 & 0 & 0 & 816 & 1840 \\ 0 & 0 & 0 & 0 & 0 & 0 & 0 & 0 & 1064 \\ 0 & 0 & 0 & 0 & 0 & 0 & 0 & 0 & 0 \end{pmatrix}.$$

2.3. *The Banded Matrices*

The constructed matrices are not suitable for numerical purposes. The inversion would be much more rapid and much more efficient if we could work on banded matrices instead of triangular ones. The operators being second-order operators on a set of orthogonal functions, there must exist a linear combination of the lines so that the matrices are reduced to banded ones (see [18]).

We exhibit here the combination we used in each domain:

• In the kernel, the Chebyshev polynomials are either odd or even, depending on the parity of l. The combination is independent of the actual value of l except for its parity.

When the Chebyshev polynomials are even we use

$$\bar{L}_i = \left(1 + \delta_0^i\right) L_i - L_{i+2} \quad (\text{for } 0 \le i \le N-3) \tag{14}$$

$$\tilde{L}_i = \bar{L}_i - \bar{L}_{i+2} \quad (\text{for } 0 \le i \le N-5) \tag{15}$$

$$\dot{L}_i = \tilde{L}_i - \tilde{L}_{i+1} \quad (\text{for } 0 \le i \le N-5) \tag{16}$$

and when they are odd we use

$$\bar{L}_i = L_i - L_{i+2} \quad (\text{for } 0 \le i \le N-3) \tag{17}$$

$$\tilde{L}_i = \bar{L}_i - \bar{L}_{i+2} \quad (\text{for } 0 \le i \le N-5) \tag{18}$$

$$\dot{L}_i = \tilde{L}_i - \tilde{L}_{i+1} \quad (\text{for } 0 \le i \le N-5), \tag{19}$$

where L_i denotes the line number i and N is the number of Chebyshev polynomials involved in the expansion. In both cases the resulting matrix is a 4-band one.

• In the shells, the basis of decomposition contains all the Chebyshev polynomials. The combination is

$$\bar{L}_i = \frac{\left(1 + \delta_0^i\right) L_i - L_{i+2}}{i+1} \quad (\text{for } 0 \le i \le N-3) \tag{20}$$

$$\dot{L}_i = \bar{L}_i - \bar{L}_{i+2} \quad (\text{for } 0 \le i \le N-5). \tag{21}$$

The resulting matrix is a 5-band one.

- In the external domain, the combination depends on the type of constructed operator.

—If the source is multiplied by r^4 the combination is

$$\overline{L}_i = \left(1+\delta_0^i\right)L_i - L_{i+2} \quad (\text{for } 0 \le i \le N-3) \tag{22}$$

$$\tilde{L}_i = \overline{L}_i - \overline{L}_{i+2} \quad (\text{for } 0 \le i \le N-5) \tag{23}$$

$$L'_i = \tilde{L}_i - \tilde{L}_{i+1} \quad (\text{for } 0 \le i \le N-5) \tag{24}$$

$$\dot{L}_i = L'_i - L'_{i+2} \quad (\text{for } 0 \le i \le N-5). \tag{25}$$

The resulting matrix is a 4-band one.

—If the source is multiplied by r^3 the combination is

$$\overline{L}_i = \left(1+\delta_0^i\right)L_i - L_{i+2} \quad (\text{for } 0 \le i \le N-3) \tag{26}$$

$$\tilde{L}_i = \overline{L}_i - \overline{L}_{i+2} \quad (\text{for } 0 \le i \le N-5) \tag{27}$$

$$\dot{L}_i = \tilde{L}_i + \tilde{L}_{i+1} \quad (\text{for } 0 \le i \le N-5). \tag{28}$$

The resulting matrix is a 4-band one.

—If the source is only multiplied by r^2, the combination is the same as the one used in the kernel for even polynomials. Thus, the resulting matrix is a 6-band one.

Of course to maintain the solution, the same linear combination is performed on the coefficients of s.

The banded matrix associated with the one presented above (in the kernel with $l = 2$ and $N = 9$) is

$$\begin{pmatrix} 0 & 0 & 56 & -336 & -200 & 0 & 0 & 0 & 0 \\ 0 & 0 & 56 & 96 & -488 & 336 & 0 & 0 & 0 \\ 0 & 0 & 0 & 144 & 168 & -672 & -504 & 0 & 0 \\ 0 & 0 & 0 & 0 & 264 & 272 & -888 & -704 & 0 \\ 0 & 0 & 0 & 0 & 0 & 416 & 408 & -1136 & -2000 \\ 0 & 0 & 0 & 0 & 0 & 0 & 600 & 1392 & 1488 \\ 0 & 0 & 0 & 0 & 0 & 0 & 0 & 816 & 1840 \\ 0 & 0 & 0 & 0 & 0 & 0 & 0 & 0 & 1064 \\ 0 & 0 & 0 & 0 & 0 & 0 & 0 & 0 & 0 \end{pmatrix}.$$

2.4. *Homogeneous Solutions*

Due to the presence of homogeneous solutions, the banded matrices are not invertible. The operator given by Eq. (7) has two homogeneous solutions which are r^l and $r^{-(l+1)}$. Those functions are eigenvectors of the matrix with the eigenvalue 0. In the kernel and the external domain, the use of the finite part of the solution can sometimes introduce other homogeneous solutions.

Let us summarize the number of such eigenvectors in each case:

- In the kernel the solution in $r^{-(l+1)}$ is singular for $r = 0$ and so is not taken into account. We have one additional homogeneous solution, arising from the finite part: T_0 for l even and T_1 for l odd.

The parity of the Chebyshev polynomials is the same as that of l so the eigen-vectors are:

—T_0 only for $l = 0$.
—T_1 only for $l = 1$.
—r^l and T_0 for $l \geq 2$, even.
—r^l and T_1 for $l \geq 3$, odd.

• In the shells we have to take into account the two usual homogeneous solutions, which are not singular in this case. We could remark that if r^l is exactly described by the Chebyshev expansion, and so implies an exact zero determinant for the matrix, it is not the case for the fractional solution $r^{-(l+1)}$. This one is not given by a finite sum of Chebyshev polynomials but rather by an infinite sum implying the result would be worse and worse as the number of coefficients increases, because the determinant of the matrix would be closer and closer to 0. So, to deal with this, we have to take into account that the eigenvalue 0 is of order 2 even if $r^{-(l+1)}$ only becomes an exact eigenvector for an infinite number of coefficients.

• In the external domain, the solution r^l is singular at infinity except for $l = 0$. $r^{-(l+1)}$ is always acceptable.

If the source is multiplied by r^4, the finite part introduces two other eigenvectors of eigenvalue 0 : T_0 and T_1. So the situation is:

—T_0 and T_1 for $l = 0$.
—T_0, T_1 and $r^{-(l+1)}$ for $l \geq 1$.

If the source is multiplied by r^3, the finite part only introduces one other eigenvector of eigenvalue 0: T_0, and the situation is:

—T_0 and $r^{-(l+1)}$ for all l.

If the source is multiplied by r^2, there are no other solutions other than the usual ones which give:

—T_0 and T_1 for $l = 0$.
—$r^{-(l+1)}$ for $l \geq 1$.

From the above discussion we are able to determine the order p of the eigenvalue 0. The banded matrices are then amputated from their p first columns and their p last lines resulting in invertible banded matrices. We abandon the p last coefficients of the source. Doing so, we find a particular solution of the system which has its p first coefficients undefined and thereafter set to zero.

In particular the previously presented matrix (in the kernel, for $l = 2$ and $N = 9$) becomes

$$\begin{pmatrix} 56 & -336 & -200 & 0 & 0 & 0 & 0 \\ 56 & 96 & -488 & 336 & 0 & 0 & 0 \\ 0 & 144 & 168 & -672 & -504 & 0 & 0 \\ 0 & 0 & 264 & 272 & -888 & -704 & 0 \\ 0 & 0 & 0 & 416 & 408 & -1136 & -2000 \\ 0 & 0 & 0 & 0 & 600 & 1392 & 1488 \\ 0 & 0 & 0 & 0 & 0 & 816 & 1840 \end{pmatrix}.$$

Before solving the system, an LU decomposition is performed using Linear Algebra Package (LAPACK) [19] for purpose of rapidity. LAPACK is also used for the resolution of the system.

2.5. *Regularity and Boundary Conditions*

In this section we will show how some homogeneous solutions are used to maintain regularity and satisfy the boundary conditions. We will concentrate on the boundary condition $f = 0$ at infinity.

• In the kernel, the operator is singular only for $l \geq 2$. If it is the case, to maintain regularity, f has to verify the following conditions:

$$f(0) = 0 \tag{29}$$

$$f'(0) = 0. \tag{30}$$

Thanks to the parity of the Chebyshev expansion, one of these conditions is always fulfilled, depending on the parity of l. So we perform a linear combination of the solution with either T_0 or T_1 to fulfill the other one. Nothing has to be done for $l \leq 1$.

• In the shells, nothing has to be done for there are neither boundary conditions nor singularities.

• In the external domain we should, once more, discriminate between three cases:

—If the source is multiplied by r^4, we must impose $f(1) = 0$ to satisfy the boundary condition; this is done by performing a linear combination of the solution and T_0. Then for $l \geq 1$, for reasons of regularity, we must have $f'(1) = 0$, a condition which is obtained by linear combination with T_1.

—In the case of a source multiplied by r^3, the boundary condition $f(1) = 0$ ensures regularity; we impose it by performing a linear combination of the solution and T_0.

—If the source is multiplied by r^2, the situation is a bit more subtle. There is no condition of regularity, but the boundary condition imposes that $f(1) = 0$. Then one can show that this implies that the source decreases as r^{-3} at infinity. Conversely, if the source decreases as r^{-3}, it implies, for $l \neq 0$, that $f(1) = 0$. So to verify boundary conditions we only consider sources decreasing as r^{-3}. It implies that the boundary condition is automatically verified for $l \neq 0$. We only impose it for $l = 0$, by doing a linear combination of the solution and T_0.

Let us emphasize that this is only the theoretical aspect of the problem. During an actual physical calculation, the sources of the Poisson equation are themselves numerically given so that they might not decrease, due to computational errors, exactly like r^{-3}. In such a case one should be cautious, for the solution will not exactly be zero at infinity. A possible treatment is to enforce the r^{-3} decay by slightly modifying the source prior to the resolution of the Poisson equation.

2.6. *Continuity*

At this stage, for each (l, m), we are left with a particular solution in each domain, one homogeneous solution in the kernel and in the external domain, and two in each shell. The last linear combination will be performed to ensure the continuity of the solution and of its first derivative across each boundary.

The simplest case is when the angular sampling is the same in every domain (i.e., the same numbers of point in θ and ϕ). The unknowns are the coefficients of the homogeneous solutions in the physical solution and the equations are given by matching f and its derivative across each boundary. It is easy to see that there is exactly the same number of equations and of unknown quantities, resulting in a uniquely determined solution.

If the angular sampling is not the same, the situation is a bit more complex; because some Y_l^m may not be present in some domains. At each boundary, for each (l, m), three situations can occur:

- the harmonic is present in the two domains: we perform the matching of both f and its derivative.
- the harmonic is present in neither domains: no equation is written.
- the harmonic is present only in one domain: we assure the continuity of f supposing that the harmonic has its coefficient equal to 0 in the domain where it is not present. We perform no matching for its derivative.

This procedure results in a system of equations that admit a unique set of solutions. We have imposed exactly as much continuity as the sampling allowed us.

To illustrate this, let us take the situation given by Table I for a specific value (l, m). In this situtation the domain 0 is the kernel and the domain 4 is the external compactified region. The column labeled Y_l^m denotes the presence or the absence of the considered spherical harmonic in each domain. The particular and homogeneous solutions are expressed taking into account the sampling and the nature of each domain. The unknowns are the coefficients of the homogeneous solutions labeled α for r^l and β for $r^{-(l+1)}$. Using the procedure described above we obtain the following equations:

- For $r = R_1$, the spherical harmonic is present in both domains, so we have to write the continuity of the solution and its derivative, which gives

$$f_0(R_1) + \alpha_0 R_1^l = f_1(R_1) + \alpha_1 R_1^l + \beta_1 R_1^{-(l+1)} \tag{31}$$

$$f_0'(R_1) + l\alpha_0 R_1^{(l-1)} = f_1'(R_1) + l\alpha_1 R_1^{(l-1)} - (l+1)\beta_1 R_1^{-(l+2)}. \tag{32}$$

- For $r = R_2$, the spherical harmonic is present only in the domain 1 and so we write only the continuity of the solution assuming that it is zero in the domain 2

$$f_1(R_2) + \alpha_1 R_2^l + \beta_1 R_2^{-(l+1)} = 0. \tag{33}$$

- For $r = R_3$, no equation is written, for the harmonic is absent on both sides of the boundary.
- For $r = R_4$, the situation is the same as at $r = R_2$

$$f_4(R_4) + \beta_4 R_4^{-(l+1)} = 0. \tag{34}$$

TABLE I

Example of the Situation before Making the Connection across Each Boundary

Domain	Bounds	Y_l^m	Particular solutions	Homogeneous solution	Unknowns
0	$0 \leq r \leq R_1$	Yes	f_0	r^l	α_0
1	$R_1 \leq r \leq R_2$	Yes	f_1	r^l and $r^{-(l+1)}$	α_1 and β_1
2	$R_2 \leq r \leq R_3$	No			
3	$R_3 \leq r \leq R_4$	No			
4	$R_4 \leq r \leq \infty$	Yes	f_4	$r^{-(l+1)}$	β_4

We have now four independent equations which are solved to find the unknowns α_0, α_1, β_1, and β_4.

All this procedure enables us to find a unique solution of the scalar Poisson equation, solution to be regular everywhere, continuous, like its derivative, and that is zero at infinity. We should point out, once more, that the source must decrease at least as r^{-3} for this to be possible.

3. CONVERGENCE PROPERTIES OF THE SCALAR POISSON EQUATION SOLVER

3.1. *Position of the Problem*

We now study the convergence of our algorithm, depending on the number of coefficients chosen for the r-expansion. The number of points for θ and ϕ does not change the precision of the result, as long as we have enough points, that is, enough spherical harmonics, to describe the source properly. However, concerning r, we perform matrix inversion and we expect a better precision as the number of coefficients increases.

It is well known (see [8, 9]) that with spectral method, the error is evanescent, i.e., decreasing as $\exp(-N)$, N being the number of coefficients, as long as we are working with functions that are $\mathcal{C}^\infty$. If the functions are only $\mathcal{C}^p$, the error is decreasing as $N^{-(p+1)}$ solely. This is known as the Gibbs phenomenon.

The various domains of our multidomain method [13] are intended to fit the surfaces of discontinuity, for example, the surface of a star (see [20] for an application to stars with discontinuous density profiles, like strange stars). Doing so, each function is $\mathcal{C}^\infty$ in each domain, removing any Gibbs phenomenon.

To test the validity of our numerical scheme, we compare calculated solutions to analytical ones. We estimate the relative error as the infinite norm of the difference over the infinite norm of the analytical solution. We will present some examples for the construction of analytical solutions. Using only $\mathcal{C}^\infty$ functions we expect errors to be evanescent.

But this is not so simple. It can be easily shown that, generally, the particular solutions obtained by the inversion of the operator for each (l, m) are of polynomial or fractional type. Those functions are exactly described by Chebyshev polynomials in r or r^{-1}. This is true except in two cases, related to the homogeneous solutions:

- a source in r^{l-2} will give rise to a particular solution in $r^l \ln r$.
- a source in $r^{-(l+3)}$ will be associated with a particular solution in $r^{-(l+1)} \ln r$.

In such cases, we expect some problems, for the description of logarithm functions in terms of Chebyshev polynomials may not be accurate. To be more precise about this effect, let us study the situation in each type of domain.

3.1.1. In the kernel. In the kernel and for reason of regularity, sources in $r^{-(l+3)}$ are obviously never present. At first glance, the case of a source in r^{l-2} seems to be more problematic, but let us recall that this source has to be the factor of Y_l^m. Can we have a source containing terms like $Y_l^m r^{l-2}$? To answer this question we refer to [10] where it is shown that, for a regular function (i.e., a function, expandable as a polynomial series in Cartesian coordinates (x, y, z) associated with (r, θ, ϕ)), terms like $r^\alpha Y_l^m$ are present in the spectral expansion only if $\alpha \geq l$. So, sources leading to a ln function in the kernel are not regular at the origin. To conclude, we expect no problem connected with particular solutions containing logarithm functions in the kernel, at least with physical regular sources.

However, let us mention the fact that if the source is the result of some calculation, it might contain some nonphysical terms due to computational errors. Those terms might give rise to some logarithmic functions.

3.1.2. In the shells. As usual there are no regularity prescriptions in the shells. The two types of particular solutions can appear. To investigate more precisely the effects of the logarithm, we studied the behavior of the error performed by expanding the two types of particular solutions in Chebyshev polynomials.

We constructed the two following exact particular solutions $r^l \ln r$ and $r^{-(l+1)} \ln r$ and approached them by a sum of Chebyshev polynomials in x, the relation between r and x being $r = \alpha x + \beta$. Then, we estimated the error by the same method as the one described previously.

Figure 1 shows an evanescent error. The functions containing logarithm are thus rather well described in a shell. This is due to the fact that the ln functions are bounded in such domains and not going to infinite values. More precisely, the $r^l \ln r$ and $r^{-(l+1)} \ln r$ functions are $\mathcal{C}^\infty$ in the shells so that the error should be evanescent. Let us mention that this result does not depend on the choice made for α and β. To conclude we expect no problem to rise from the presence of such particular solutions in the shells.

3.1.3. In the external compactified domain. The particular solution in $r^l \ln r$ is not going to zero at infinity and so cannot appear in the external domain. But the other type of particular solution $r^{-(l+1)} \ln r$ is likely to appear. We investigate the effect by the same method as the one used in the shells, that is, determining the behavior of the error made by interpolating the exact solution by a finite sum of Chebyshev polynomials.

Figure 2 shows that the error is no longer evanescent but follows a power law. The error is decreasing faster and faster as l increases, because the associated particular solution is being

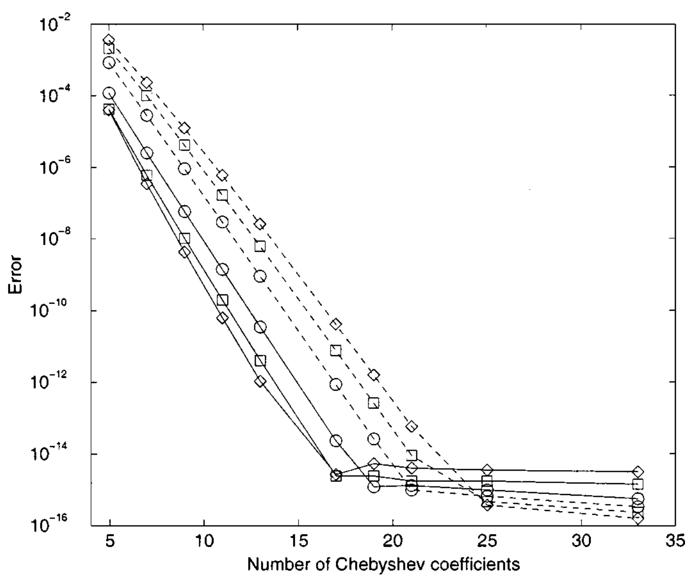

FIG. 1. Relative difference (infinite norm) between the particular solutions with logarithm and their truncated Chebyshev expansions, in a shell. The scale for the number of coefficients is linear. The solid lines represent the $r^l \ln r$ functions and the dashed lines the $r^{-(l+1)} \ln r$ ones. The circles represent the case $l = 0$, the squares $l = 1$, and the diamonds $l = 2$. This plot has been obtained using $\alpha = 0.5$ and $\beta = 1.5$.

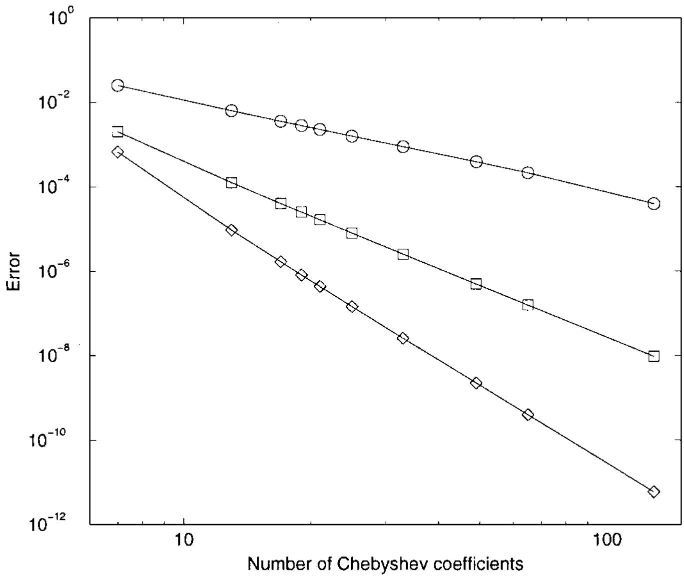

FIG. 2. Relative difference (infinite norm) between the particular solutions with logarithm and their truncated Chebyshev expansions, in the external domain. The scale for the number of coefficients is logarithmic. The circle represent the case $l = 0$, the squares $l = 1$, and the diamonds $l = 2$.

better approached by Chebyshev polynomials. In other words, the function $r^{-(l+1)} \ln r = -u^{(l+1)} \ln u$ is not $\mathcal{C}^\infty$, for its $(l+1)$ derivative contains terms in $\frac{1}{u}$, not regular at spatial infinity, that is for $u = 0$. More precisely, Fig. 3 shows the value of the exponent as a function of l.

We can conclude that the error made by expanding $r^{-(l+1)} \ln\, r$ Chebyshev polynomials follows a power law and that it is decreasing faster than $N^{-2(l+1)}$. We will use this to explain some features of our scalar and vectorial Poisson equation solvers.

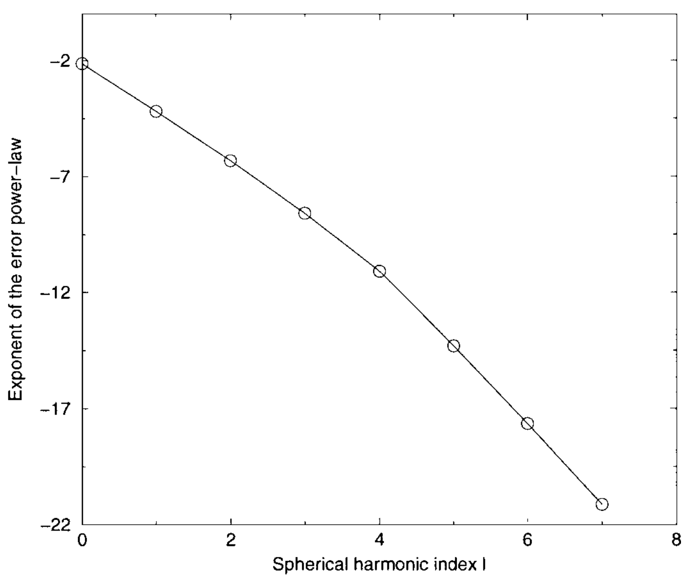

FIG. 3. Exponent of the power law followed by the error shown in Fig. 2, as a function of l.

3.2. *Accuracy Estimated by Comparison with Analytical Solutions*

From the results of the previous section, we expect an evanescent error for the resolution of the scalar Poisson equation when there is no particular solution containing any logarithm in the external domain and an error follows a power law when such solution do appear. We present here some results that illustrate this behavior and lead to two properties about the error.

3.2.1. Spherically symmetric source. First of all, let us consider a simple case for which we do not expect any Gibbs-like phenomenon: a spherically symmetric source decreasing as r^{-4}. In fact, the only harmonic present in this source is $l = 0$, which would imply a ln solution only for a source in r^{-3}. We choose a source S decreasing as r^{-4} in the external domain and a polynomial one, such that the solution is not singular in the kernel. The associated solution F can be found analytically.

In the external domain, for $r > R$, we have

$$S = \frac{R^5}{r^4}; \quad F = \frac{R^5}{2r^2} - \frac{17}{15}\frac{R^4}{r}, \tag{35}$$

and for $r < R$,

$$S = R - \frac{r^2}{R}; \quad F = \frac{Rr^2}{6} - \frac{r^4}{20R} - \frac{3}{4}R^3. \tag{36}$$

As expected Fig. 4 shows an evanescent error, with some saturation at the level of 10^{-15} due to the round-off error, the calculation being performed in double precision. No significant difference can be seen between the three schemes.

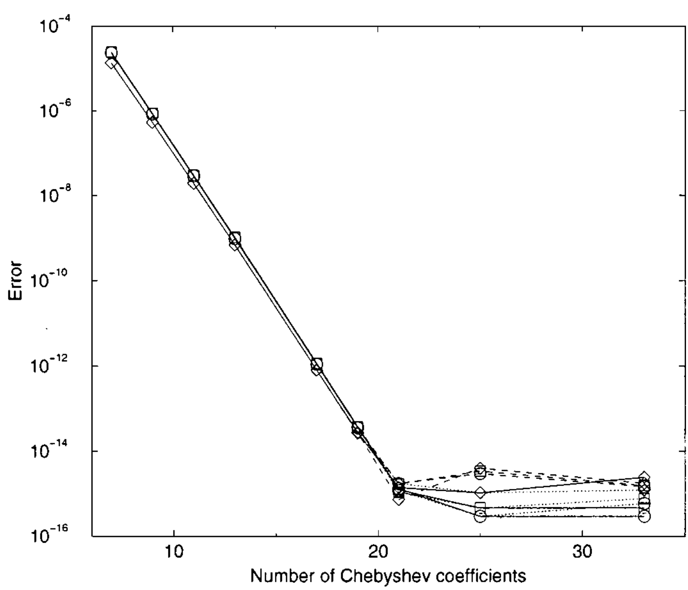

FIG. 4. Error on the resolution of the scalar Poisson equation for a spherically symmetric source extending to infinity. The solid lines represent the $r^4 S$ scheme, the dotted lines the $r^3 S$ scheme, and the dashed lines the $r^2 S$ one. The scale for the number of coefficients is linear. The circles represent the error in the kernel, the squares in the shell, and the diamonds in the external domain.

3.2.2. Compact source. Another interesting case is that of a source with a compact support, that is, a source which is zero in the external domain. As for the previous case we do not expect any Gibbs phenomenon. In the external domain let us choose the following analytical solution

$$F = Y_l^0 \frac{1}{r^{l+1}}. \tag{37}$$

This solution leads to a source that vanishes in the external domain. To avoid any singularity at the center, we choose the latter function as a solution of the equation for $r < R$

$$F = Y_l^0 \left[(2l+5) \frac{r^2}{2R^{2l+3}} - (2l+3) \frac{r^4}{2R^{2l+5}} \right]. \tag{38}$$

This solution has been chosen so that F and its first derivative with respect to r are continuous at $r = R$, properties of the solution given by our algorithm. The associated source, for $r < R$, is found by taking the Laplacian of F

$$S = Y_l^0 \left[(2l+5)(2l+3) \frac{1}{R^{2l+3}} - (2l+3)(4l+10) \frac{r^2}{R^{2l+5}} \right]. \tag{39}$$

So we constructed a nonspherically symmetric compact source, which contains only one spherical harmonic. We chose for simplicity $m = 0$, because we do not expect any variation with m, the latter than being absent of the inverted operator.

As expected, Fig. 5 shows an evanescent error down to a saturation value of approximatively 10^{-14}.

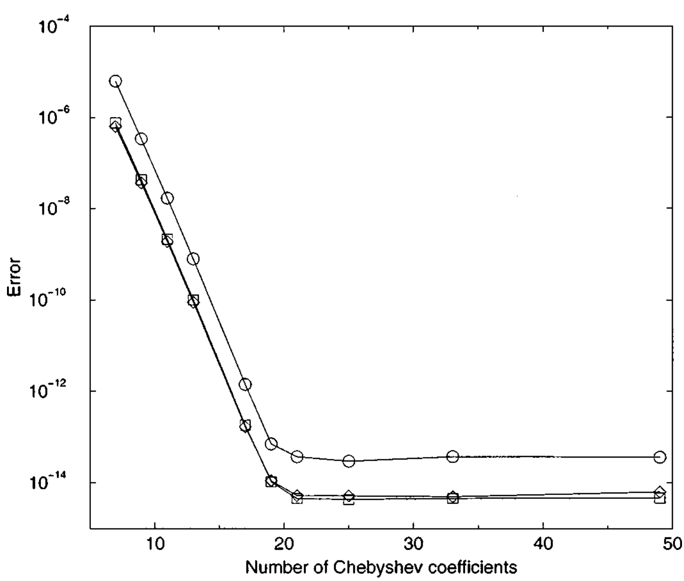

FIG. 5. Error on the resolution of the Poisson-like equation for a nonspherical compact source with $l = 2$. The scale for the number of coefficients is linear. The circles represent the error in the kernel, the squares in the shell, and the diamonds in the external domain.

3.2.3. A logarithm in a shell. The last case with an evanescent error we considered is the one where the problematic particular solutions (i.e., containing a logarithm) appear only in a shell bounded by $R_1 < r < R_2$. We choose a source s that implies the appearance of both types of particular solutions. Let F be the associated solution. In the shell, for $R_1 < r < R_2$, we have

$$
\begin{aligned}
S_{\text{shell}} &= \frac{1}{r^3} + 3\frac{z^2}{r^2} - 1 \\
F_{\text{shell}} &= -\frac{\ln r}{r} + \frac{\ln R_1 - 1}{r} + \frac{1}{R_2} + \left(3\frac{z^2}{r^2} - 1\right)\left(\frac{1}{5}r^2 \ln r - \left(\frac{\ln R_2}{5} + \frac{1}{25}\right) r^2 + \frac{R_1^5}{25}\frac{1}{r^3}\right)
\end{aligned}
\tag{40}
$$

For simplicity, we take $S = 0$ in the kernel and in the external domain, the solution being chosen, once more, by continuity across the boundaries

$$
\begin{aligned}
F_{\text{kernel}} &= \frac{1}{R_2} - \frac{1}{R_1} + \frac{\ln R_1 - \ln R_2}{5} r^2 \left(3\frac{z^2}{r^2} - 1\right) \\
F_{\text{external}} &= \frac{\ln R_1 - \ln R_2}{r} + \frac{1}{r_3}\frac{R_1^5 - R_2^5}{25}\left(3\frac{z^2}{r^2} - 1\right).
\end{aligned}
\tag{41}
$$

The result presented in Fig. 6 shows an evanescent error, confirming that the presence of a logarithm function is only a problem in the external domain. Once more let us mention that this is due to the fact that the logarithm functions are bounded in a shell and not going to infinite values. Such bounded functions are rather well described in terms of Chebyshev polynomials.

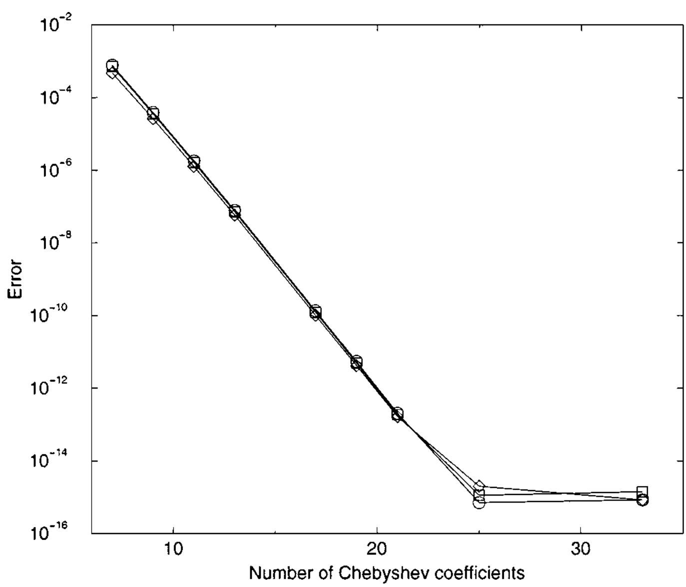

FIG. 6. Error on the resolution of the scalar Poisson equation for a solution containing bounded logarithm functions. The scale for the number of coefficients is linear. The circles represent the error in the kernel, the squares in the shell, and the diamonds in the external domain.

3.2.4. The Gibbs phenomenon. Let us now consider a case where the particular solution contains a logarithm in the external domain. Following the construction of the source and solution in Section 3.2.2 let us take the following source in the external domain.

$$S = -Y_l^0 \frac{1}{r^{l+3}}, \tag{42}$$

and $S = 0$ for $r < R$. The associated unique solution is

$$\begin{aligned} F &= Y_l^0 \frac{r^l}{(2l+1)^2 R^{2l+1}} \quad \text{for } r < R \\ F &= Y_l^0 \frac{\ln(r) - \ln(R) + \frac{1}{2l+1}}{(2l+1) r^{l+1}} \quad \text{for } r > R. \end{aligned} \tag{43}$$

Figure 7 presents an example of the obtained results for each of the three schemes discussed in Section 2.2. A logarithm being present in the solution, the error is no longer evanescent and it follows a power law. One important feature is that the $r^4 S$ scheme is converging much less rapidly than the $r^3 S$ and $r^2 S$ ones. This may be due to the fact that for a given source, the $r^4 S$ scheme is dealing with particular solutions less rapidly decreasing.

In Fig. 8 the slope of the power law is plotted as a function of the harmonic index l, for the three different schemes. It reveals an error decreasing as $N^{-2(l+1)}$ for the $r^2 S$ and $r^3 S$ schemes and as N^{-2l} for the $r^4 S$ one. Let us mention that the $r^2 S$ scheme yields an error following the same power law as the one rising from the description of the associated function (cf. Section 3.1.3), making us confident about the origin of such a behavior.

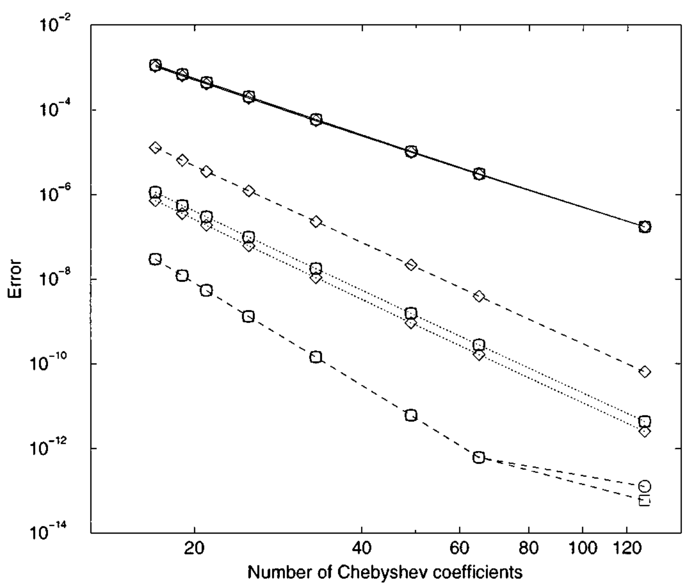

FIG. 7. Error on the resolution of the scalar Poisson equation for a solution containing ln functions for $l = 2$. The scale for the number of coefficients is logarithmic. The circles represent the error in the kernel, the squares in the shell, and the diamonds in the external domain. Solid lines represent the scheme with $r^4 S$, the dotted ones the scheme with $r^3 S$, and dashed lines the scheme with $r^2 S$.

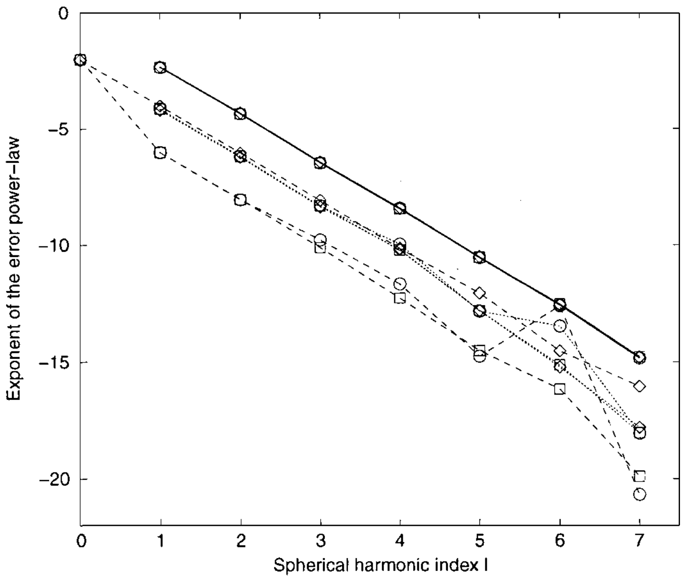

FIG. 8. Exponent of the power law followed by the error shown in Fig. 7 as a function of the index l. The solid lines correspond to the r^4S scheme, the dotted lines to the r^3S scheme, and the dashed lines to the r^2S scheme. The circles represent the error in the kernel, the squares in the shell, and the diamonds in the external domain.

3.3. *Convergence Properties*

All the examples shown in the previous section enable us to propose the two following empirical properties concerning the decrease of the error.

Property 1. If the source is decreasing as r^{-k} at infinity and does not contain any spherical harmonics with $l \geq k-3$, then the error is evanescent.

Property 2. If the source decrease at least as r^{-k} at infinity, then the error decreases at least as $N^{-2(k-2)}$ (resp. N^{-2k}) for the r^2S and r^3S schemes (resp r^4S scheme).

The first property is just issued from the presence of a ln function in the external domain and the second property comes from the values of the power law found in the previous section.

4. VECTORIAL POISSON EQUATION

Using the Poisson equation solver from Section 2 and studied in Section 3, we focus now on the vectorial Poisson equation given by Eq. (2), in the nondegenerated case (i.e., $\lambda \neq -1$).

Let us first mention that the operator $\Delta + \lambda\vec{\nabla}(\vec{\nabla}\cdot)$ has been shown to be strongly elliptic and self-adjoint in [5, 6] in the case $\lambda = 1/3$ (conformal Laplace operator). Conditions for existence and uniqueness of solutions have been presented in Appendix B of [4]. The harmonic vectorial functions of this operator and the associated multipole expansions have been discussed by Ó Murchadha [21].

Three different schemes have been previously proposed by other authors [14–16] to reduce the resolution of Eq. (2) to those of four scalar Poisson equations. Let us emphasize that those three schemes are not covariant. They are only applicable in Cartesian coordinates which allow us to commute operators like Laplacian and gradient.

Let us mention the fact that a different method, based on solving for the degenerated case (i.e., $\lambda = 1$) has been proposed in [10] but is not studied in the present work.

4.1. *The Bowen–York Method*

The idea of this method (see [14]) is to search for the solution of Eq. (2) in the form

$$\vec{N} = \vec{W} + \vec{\nabla}\chi, \tag{44}$$

where $\vec{W}$ and χ are solutions of

$$\Delta\vec{W} = \vec{S} \tag{45}$$

$$\Delta\chi = -\frac{\lambda}{\lambda+1}\vec{\nabla}\cdot\vec{W}. \tag{46}$$

This method gives a solution to Eq. (2) but let us check that this solution is the one that is $\mathcal{C}^1$. $\vec{W}$ is $\mathcal{C}^1$, being a solution of a Poisson equation. This implies that the source of the equation for χ is continuous, and that χ is $\mathcal{C}^2$. This is sufficient to ensure that $\vec{N}$ is $\mathcal{C}^1$. The scheme finds the only solution $\mathcal{C}^1$ and one going to zero at infinity.

Unfortunately this very simple method is not applicable with our Poisson equation solver, because the physical sources are not decreasing fast enough at infinity. For the problem that motivated this study, namely binary neutron star systems [22, 23], the source $\vec{S}$ of Eq. (2) is expected to behave like r^{-4} at infinity implying that we can calculate $\vec{W}$. This vector field is acting like r^{-1} at infinity, because r^{-1} is a homogeneous solution of the scalar Poisson equation usually present (monopolar term).

So the source of the equation for χ, being the divergence of $\vec{W}$, behaves like r^{-2}. This decreasing is not fast enough to compute the value of χ. Analytically no problem occurs because only the gradient of χ is relevant, not χ itself, for the calculation of the solution. To summarize, the implementation of this scheme conducts to the computation of diverging quantities, making the result wrong in the external domain. We should say that this scheme is applicable for domains not extending to infinity. However, it may be possible to use it by treating analytically the diverging quantities.

4.2. *The Oohara–Nakamura Method*

In this case (see Section 3.1.1 of [15]) we start by solving the following scalar equation

$$\Delta\chi = \frac{1}{\lambda+1}\vec{\nabla}\cdot\vec{S}. \tag{47}$$

Then the solution of Eq. (2) is found by solving the following set of three equations

$$\Delta\vec{N} = \vec{S} - \lambda\vec{\nabla}\chi. \tag{48}$$

Comparing (2) with (48) shows that this scheme gives the exact solution of Eq. (2) if and only if

$$\vec{\nabla}\chi = \vec{\nabla}(\vec{\nabla}\cdot\vec{N}). \tag{49}$$

But the scalar equation (47) only ensures that

$$\Delta(\chi - \vec{\nabla} \cdot \vec{N}) = 0. \tag{50}$$

From Section 2, we can show that it is possible to construct a homogeneous solution of the scalar Poisson equation, in all spaces that is nonzero, going to zero at infinity, if and only if that solution is not $\mathcal{C}^1$.

In the general case, $\vec{\nabla} \cdot \vec{N}$ is only $\mathcal{C}^0$ at the boundary between the different domains, while χ, solution of a Poisson equation, is $\mathcal{C}^1$. So it is possible to fulfill Eq. (50) and not Eq. (49). If $\vec{\nabla} \cdot \vec{N}$ is $\mathcal{C}^1$, then Eq. (50) implies, as shown in Section 2, that $\chi = \vec{\nabla} \cdot \vec{N}$. In this case, the condition (49) is trivially fulfilled. Imposing that $\vec{\nabla} \cdot \vec{N}$ is at least $\mathcal{C}^1$ is equivalent to imposing that $\vec{S}$ is continuous across every boundary.

To conclude, let us say that the Oohara–Nakamura method gives the exact solution if and only if the source $\vec{S}$ is continuous across every boundary delimiting the different domains. This property is general, meaning that it is not due to our numerical method. We can mention that the found solution is the $\mathcal{C}^1$ one, because it is calculated as solution of three scalar Poisson equations.

Next let us see if this scheme is applicable, using our scalar Poisson equation solver. At first glance this scheme suffers the same drawback as the Bowen–York scheme. Because of homogeneous solutions of the scalar Poisson equation, χ is decreasing as r^{-1} at infinity and its gradient as r^{-2}, which is not enough to allow us to solve the set (48) of three scalar Poisson equations.

The difference is that the solution of Eq. (48) is the solution of the vectorial Poisson equation (2) and we must be able to set it to zero at infinity, contrary to the Bowen–York method where the problem occurs for auxiliary quantities.

So it must be possible to show that the source of Eq. (48) decreases fast enough, that is, at least as r^{-3}. The problem arises from the monopolar term of χ, i.e., the only one that gives an homogeneous solution in r^{-1} in the external domain. It is known, that the monopolar term M_0 of the solution of a scalar Poisson equation with source σ, is given by

$$M_0 = \frac{1}{4\pi} \iiint \sigma \, \mathrm{d}^3 r, \tag{51}$$

the integration being performed over all spaces.

Now we have $\sigma = \vec{\nabla} \cdot \vec{S}$. The use of Green formula leads to

$$M_0 = \frac{1}{4\pi} \iint \vec{S} \cdot \mathrm{d}\vec{s}, \tag{52}$$

the surface integration being done at infinity. But $\vec{S}$ decreases as r^{-4}, implying that the surface integral is zero, that is, $M_0 = 0$. This remains true if the source acts only like r^{-3}.

So the monopolar term of χ is zero, which implies that χ decreases at least as r^{-2}. This behavior ensures that the source of Eq. (48) decreases as r^{-3}, allowing us to find the unique solution going to zero at infinity.

We implemented and tested this scheme, recalling that it is only applicable if the source of Eq. (2) is continuous and requires that the source decreases at least like r^{-3} at infinity.

4.3. *The Shibata Method*

The solution is now found as (see [16])

$$\vec{N} = \frac{1}{2}\frac{\lambda + 2}{\lambda + 1}\vec{W} - \frac{1}{2}\frac{\lambda}{\lambda + 1}(\vec{\nabla}\chi + \vec{\nabla}\vec{W}\cdot\vec{r}), \tag{53}$$

where $\vec{W}$ and χ are solutions of

$$\Delta\vec{W} = \vec{S} \tag{54}$$

$$\Delta\chi = -\vec{r}\cdot\vec{S}. \tag{55}$$

and $\vec{r}$ denotes the vector of coordinates (x, y, z).

This scheme gives a solution to Eq. (2), but, as with the Bowen–York method, let us quickly check that it is the unique $\mathcal{C}^1$ going to zero at infinity. At infinity, $\vec{W}$, a solution of scalar Poisson equation, is behaving at least like r^{-1}. This ensures that $\vec{\nabla}\vec{W}\cdot\vec{r}$ is zero at infinity, proving that the solution goes to zero.

Concerning the continuity, being solutions of scalar Poisson equations, we know that both $\vec{W}$ and χ are at least $\mathcal{C}^1$. But we have to take care of the term $\vec{\nabla}\chi + \vec{\nabla}\vec{W}\cdot\vec{r}$ of Eq. (53). First we can show that

$$\Delta(\vec{r}\cdot\vec{W}) = \vec{r}\cdot\vec{S} + 2\vec{\nabla}\cdot\vec{W}. \tag{56}$$

Using that property and the equation for χ we can see that

$$\Delta(\vec{r}\cdot\vec{W} + \chi) = 2\vec{\nabla}\cdot\vec{W}. \tag{57}$$

The source of that equation is $\mathcal{C}^0$, so that $\vec{r}\cdot\vec{W} + \chi$ is $\mathcal{C}^2$. The term of Eq. (53), can be expressed as

$$\vec{\nabla}\chi + \vec{\nabla}\vec{W}\cdot\vec{r} = \nabla(\vec{r}\cdot\vec{W} + \chi) - \vec{W}. \tag{58}$$

Using the continuity properties found above, it is easy to see that the right-hand side of Eq. (58) is $\mathcal{C}^1$, which ends our demonstration by proving that the calculated $\vec{N}$ is $\mathcal{C}^1$.

As before, let us now check if this method is applicable by means of our scalar Poisson equation solver. The source of the equation for χ decreases at least like r^{-3} at infinity if and only if $\vec{S}$ decreases like r^{-4}. Like the Oohara–Nakamura scheme, this scheme does not involve any diverging quantities and so is suitable for numerical purposes.

This method has been implemented and, contrary to the Oohara–Nakamura method, can be used even with discontinuous source, but requires that $\vec{S}$ decreases at least like r^{-4} at infinity, which, let us recall, is the case for the physical problems we intend to study.

4.4. *Convergence Criterion*

As seen before the resolution of Eq. (2) reduces to that of four scalar Poisson equations. So we should be able to use the results of Section 3.3 to establish a convergence criterion for the schemes proposed in [15, 16].

4.4.1. The Oohara–Nakamura scheme. Let us suppose that the source $\vec{S}$ of Eq. (2) contains only one spherical harmonic Y_l^m and decreases as r^{-k} at infinity ($k \geq 3$).

For the Oohara–Nakamura method, the source of the first Poisson equation is $\vec{\nabla} \cdot \vec{S}$: the degree of the harmonic is $l+1$ and the decrease is as $r^{-(k+1)}$. These two effects are opposed concerning the convergence properties established in Section 3.3. So, in the case where no logarithm appears during the calculation to find χ, χ contains one spherical harmonic $l+1$ and decreases as $r^{-(k-1)}$ and so $\vec{\nabla}\chi$, part of the source of Eq. (48), contains one spherical harmonic with $l+2$ and acting like r^{-k} at infinity. So the conditions for the appearance of a Gibbs-like phenomenon are "harder" by two degrees than for a scalar Poisson equation and occurs for a source with a spherical index $l+2$.

4.4.2. The Shibata scheme. Suppose we consider the same source as in the previous section. The convergence properties for the equation for $\vec{W}$ are the same as those for a usual scalar Poisson equation.

Concerning the equation for χ the source is $-\vec{r} \cdot \vec{S}$. Performing such an operation on $\vec{S}$ increases the degree of the spherical harmonics by one unit. At the same time, the decrease of the source is slower, due to multiplication by r everywhere. Those two phenomena have the same effect on the convergence criterion we previously established. As for the Oohara–Nakamura scheme, the criteria are "harder" by two degrees but the Gibbs-like phenomenon occurs for a source in $l+1$.

4.4.3. Convergence properties. We are now able to deduce convergence properties for the two schemes. From the study above, we can see that if the condition for the appearance of the Gibbs-like phenomenon is the same, it is not associated with the same index l. This results in the two following properties:

Property 1. If the source of a vectorial Poisson equation is decreasing as r^{-k} at infinity ($k \geq 3$ for the Oohara–Nakamura scheme and $k \geq 4$ for the Shibata scheme) and does not contain any spherical harmonics with $l \geq k-5$, then the error is evanescent.

Property 2. If the source decreases at least as r^{-k} at infinity then the error is decreasing at least as $N^{-2(k-2)}$ for the Oohara–Nakamura method ($k \geq 3$) and at least as $N^{-2(k-3)}$ for the Shibata method ($k \geq 4$).

5. ACCURACY OF THE VECTORIAL POISSON EQUATION SOLVERS ESTIMATED BY COMPARISON WITH ANALYTICAL SOLUTIONS

To check the validity of the schemes and their convergence, we used the same method as that used for the scalar Poisson equation, that is, the use of analytical solutions of various properties. The solutions associated with the sources have been obtained by following analytically the Shibata scheme.

5.1. *Continuous Source*

Let us consider the case of a continuous source extending to infinity, say, for example, in the external compactified domain, for $r > R$

$$S^x = \frac{x}{r^{n+5}}; \quad S^y = \frac{y}{r^{n+5}}; \quad S^z = \frac{z}{r^{n+5}} \tag{59}$$

and for $r < R$

$$S^x = \frac{x}{R^{n+5}}; \quad S^y = \frac{y}{R^{n+5}}; \quad S^z = \frac{z}{R^{n+5}}. \tag{60}$$

Note that this source is $\mathcal{C}^0$, the minimum requirement for the Oohara–Nakamura method to be applicable.

For $n \neq 0$, the associated solution in the external domain is

$$N^x = \frac{1}{(\lambda+1)n(n+3)} \frac{x}{r^{n+3}} - \frac{n+5}{(\lambda+1)15n} \frac{x}{R^n r^3} \tag{61}$$

and for $r < R$

$$N^x = \frac{1}{10(\lambda+1)} \frac{xr^2}{R^{n+5}} - \frac{n+5}{(\lambda+1)6(n+3)} \frac{x}{R^{n+3}}. \tag{62}$$

the other components being obtained by permutation of x, y and z.

For $n \neq 0$ no Gibbs-like phenomenon occurs by solving the equations with $\vec{S}$ as source. For $n \leq 2$, a Gibbs-like phenomenon should appear due to the vectorial nature of Eq. (2). This is not the case because of simplifications due to the symmetry of the source. It just shows that the two convergence criteria established above are rather pessimistic. The evanescent error is shown in Fig. 9. As for the scalar case, a saturation is attained at a level of approximately 10^{-11}.

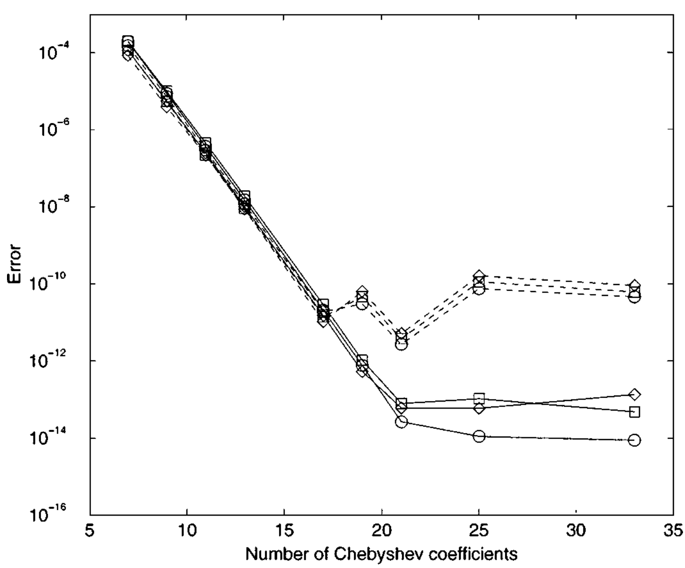

FIG. 9. Error on the z component for a continuous source extending to infinity (Eqs. (59) and (60) with $n = 1$). The scale for the number of coefficients is linear. The solid lines represent the Shibata scheme and the dashed lines the Oohara–Nakamura scheme. The circles represent the error in the kernel, the squares in the shell, and the diamonds in the external domain.

5.2. *A Vectorial Gibbs-like Phenomenon*

At this point, we exhibit an analytical solution that produces a Gibbs-like phenomenon which arises from the vectorial nature of Eq. (2). Let us consider the following source

$$S^z = \frac{z}{r^7} \tag{63}$$

in the external compactified domain, and for $r < R$

$$S^z = \frac{z}{R^7}. \tag{64}$$

We set the two other components to zero in all spaces.

If we solve the scalar Poisson equation with S^z as source, the error will be evanescent, as shown in Section 3.3. But, according to the conclusion we obtained concerning the convergence criterion of a vectorial Poisson equation, a Gibbs-like phenomenon should appear due to the vectorial nature of Eq. (2).

In the external domain, the associated solution is

$$\begin{aligned}
N^x &= -\frac{1}{2}\frac{\lambda}{\lambda+1}\left[\frac{z^2x}{r^7}\left(-\frac{9}{14}+\ln(R)-\ln(r)\right)+\frac{7}{10}\frac{z^2x}{r^5R^2}\right.\\
&\quad\left.+\frac{x}{r^5}\left(\frac{59}{350}+\frac{\ln(r)-\ln(R)}{5}\right)-\frac{7}{30}\frac{x}{r^3R^2}\right]\\
N^y &= -\frac{1}{2}\frac{\lambda}{\lambda+1}\left[\frac{z^2y}{r^7}\left(-\frac{9}{14}+\ln(R)-\ln(r)\right)+\frac{7}{10}\frac{z^2y}{r^5R^2}\right.\\
&\quad\left.+\frac{y}{r^5}\left(\frac{59}{350}+\frac{\ln(r)-\ln(R)}{5}\right)-\frac{7}{30}\frac{y}{r^3R^2}\right]\\
N^z &= \frac{1}{2}\frac{\lambda+2}{\lambda+1}z\left(\frac{1}{10r^5}-\frac{7}{30}\frac{1}{r^3R^2}\right)-\frac{1}{2}\frac{\lambda}{\lambda+1}\left[\frac{z^3}{r^7}\left(-\frac{9}{14}+\ln(R)-\ln(r)\right)\right.\\
&\quad\left.+\frac{7}{10}\frac{z^3}{R^2r^5}+\frac{z}{r^5}\left(\frac{3}{5}(\ln(r)-\ln(R))+\frac{71}{175}\right)-\frac{7}{15}\frac{z}{r^3R^2}\right]
\end{aligned} \tag{65}$$

and for $r < R$, we found

$$\begin{aligned}
N^x &= -\frac{1}{2}\frac{\lambda}{\lambda+1}x\left(\frac{2}{35}\frac{z^2}{R^7}+\frac{1}{35}\frac{r^2}{R^7}-\frac{7}{75}\frac{1}{R^5}\right)\\
N^y &= -\frac{1}{2}\frac{\lambda}{\lambda+1}y\left(\frac{2}{35}\frac{z^2}{R^7}+\frac{1}{35}\frac{r^2}{R^7}-\frac{7}{75}\frac{1}{R^5}\right)\\
N^z &= \frac{1}{2}\frac{\lambda+2}{\lambda+1}z\left(\frac{1}{10}\frac{r^2}{R^7}-\frac{7}{30}\frac{1}{R^5}\right)-\frac{1}{2}\frac{\lambda}{\lambda+1}z\left(\frac{2}{35}\frac{z^2}{R^7}-\frac{1}{70}\frac{r^2}{R^7}-\frac{7}{150}\frac{1}{R^5}\right).
\end{aligned} \tag{66}$$

As expected, Fig. 10 shows an error obeying a power law. This feature is more evident in the external domain where the particular solution is directly present. The Gibbs-like phenomenon appears for the two schemes. Let us apply Property 2 to determine the exponent of the power law. The source of the equation decreases as r^{-6}. This implies that the error for the Oohara–Nakamura scheme should decrese at least as N^{-8} and as N^{-6} for the Shibata scheme. This is well confirmed for the Shibata scheme which exhibits an exponent –6.4.

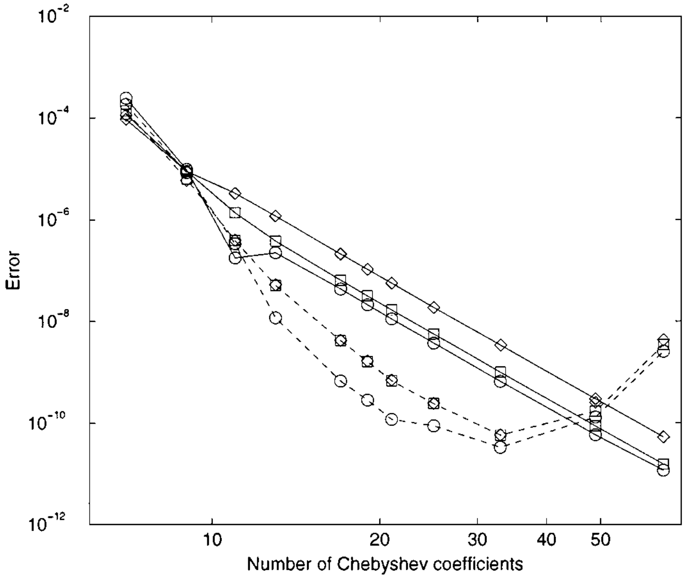

FIG. 10. Error on the z component for a source implying a Gibbs-like phenomenon. The scale for the number of coefficients is logarithmic. The solid lines represent the Shibata scheme and the dashed lines the Oohara–Nakamura scheme. The circles represent the error in the kernel, the squares in the shell, and the diamonds in the external domain.

For the Oohara scheme it turns out that the criterion is rather pessimistic because the error decreases faster than N^{-12}.

5.3. *A Discontinuous Source*

As previously explained, the Oohara–Nakamura scheme fails to solve Eq. (2) in the case of a discontinuous source. We will now consider such a source and show that the Shibata method is efficient, even in such a case.

In the compactified domain, $r > R$, we choose the following solution

$$N^x = \frac{x}{r^n}. \tag{67}$$

For $r < R$, we ensure the continuity of the solution and its derivative by choosing

$$N^x = x(ar^6 + br^4), \tag{68}$$

where $a = -\frac{4+n}{2R^{n+6}}$ and $b = \frac{6+n}{2R^{n+4}}$. The associated source is obtained by calculating the left-hand side of Eq. (2). In the external domain we obtain

$$\begin{aligned} S^x &= n(n-3-3\lambda)\frac{x}{r^{n+2}} + n(n+2)\lambda\frac{x^3}{r^{n+4}} \\ S^y &= -\lambda n\frac{y}{r^{n+2}} + n(n+2)\lambda\frac{x^2y}{r^{n+4}} \\ S^z &= -\lambda n\frac{z}{r^{n+2}} + n(n+2)\lambda\frac{x^2z}{r^{n+4}} \end{aligned} \tag{69}$$

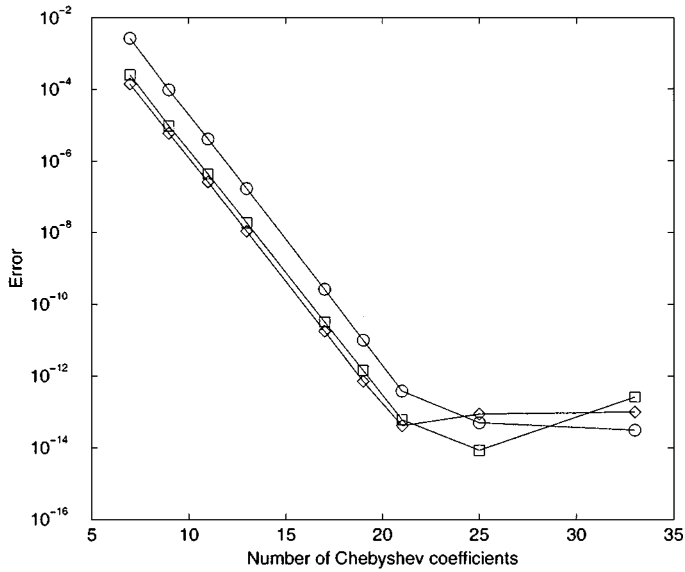

FIG. 11. Error on the x component for discontinuous source (Eqs. (69) and (70) with $n = 4$). The scale for the number of coefficients is linear. The circles represent the error in the kernel, the squares in the shell, and the diamonds in the external domain.

and for $r < R$, we have

$$\begin{aligned} S^x &= x[(54 + 18\lambda)ar^4 + (28 + 12\lambda)br^2] + \lambda x^3(24ar^2 + 8b) \\ S^y &= \lambda y[6ar^4 + 4br^2 + x^2(24ar^2 + 8b)] \\ S^z &= \lambda z[6ar^4 + 4br^2 + x^2(24ar^2 + 8b)]. \end{aligned} \tag{70}$$

Depending on the value of n, the error may or may not be evanescent. Only a few spherical harmonics are present in the source and we can show that we expect, for example, an evanescent error for $n = 4$ and a Gibbs phenomenon for $n = 5$. This might seem not to be in agreement with the convergence criterion previously established, but recall that it is rather general and much more pessimistic to handle simple sources such as the ones considered here.

The results presented in Figs. 11 and 12 show that the discontinuity of the source has no effect on the resolution of the vectorial Poisson equation, as long as the Shibata scheme is used. For $n = 5$, the source is like r^{-6} at infinity and we expect an error decreasing more rapidly than N^{-6}. Figure 12 shows an extremely good agreement with the prediction, because the power law exhibits an exponent of –6.4.

6. DEVELOPMENTS

In this section we present some extension of this work that is solving more complicated equations using the schemes presented here as milestones.

The first extension that has been conducted regards nonspherical domains, with spheroidal shapes (i.e., they must have the same topology as a sphere). This is very useful for we can define the boundary of each domain to match with surfaces of discontinuity, like stellar

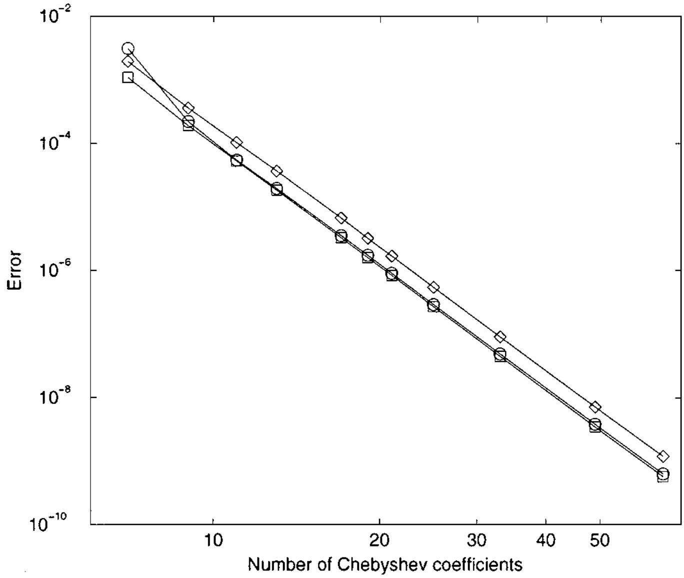

FIG. 12. The error is the same as in Fig. 11 but for $n = 5$; the scale for the number of coefficients is now logarithmic.

surfaces, so that each field is $\mathcal{C}^\infty$ in each domain preventing any Gibbs phenomenon. Thanks to some mapping onto a sphere, solving the Poisson equations with such boundaries reduces to the spherical case, with correction terms appearing in the source. The equation is then solved by iteration. The method is described in detail in [13]. In that paper the calculation of the Mac–Laurin and of the Roche ellipsoids have been compared with the analytical solutions. The behavior of the error when one increases the number of coefficients happens to be evanescent (see Figs. 5 and 6 of [13]). Those calculations being made in the Newtonian case, all the sources are compactly supported. This shows that the nonsphericity does not introduce any new Gibbs phenomenon with respect to the spherical case.

Concerning calculations in general relativity (i.e., with sources extending to infinity), results have been obtained for rapidly rotating strange stars in [20] using nonspherical domains. Convergence properties have not been fully explored, because there exists no analytical solution to compare with. Anyway, we can suppose that with the sources containing almost every spherical harmonic, the convergence will no longer be evanescent but will rather follow a power law.

Another important extension of this work deals with two bodies, for example, orbiting binary neutron stars. This case has been successfully studied in [22, 23] by means of the Poisson solvers presented here. The main difference with the cases we discussed in the present paper is that the sources are no longer spheroidal but are concentrated on two spheroidal domains being the two stars. An equation of type (1) is then split into two parts

$$\begin{aligned} \Delta F_1 &= S_1 \\ \Delta F_2 &= S_2, \end{aligned} \tag{71}$$

where the real source is $S = S_1 + S_2$. We use two sets of spherical coordinates, one centered on each star and the splitting is done so that S_1 is mainly centered on the first star and S_2

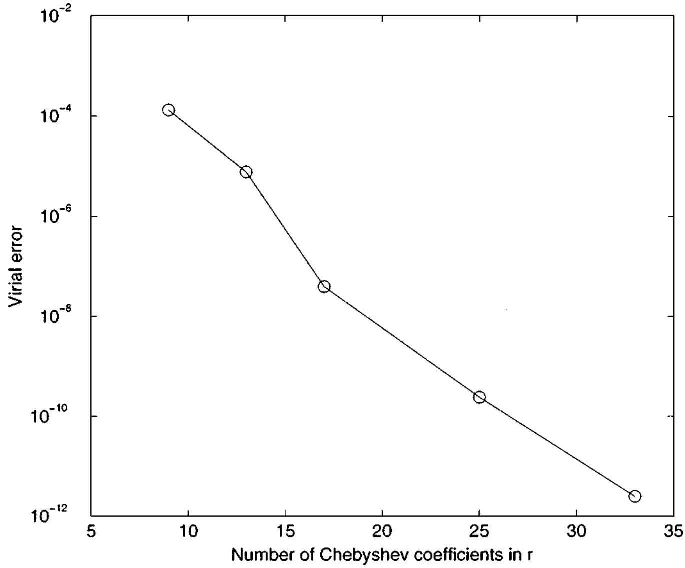

FIG. 13. Relative error, estimated by means of the virial theorem, for a Newtonian irrotational binary star calculation with respect to the number of Chebyshev coefficients.

on the other star (see [23] for details). The sources S_i are then well described in spheroidal topology and the total equation is well solved, the solution being $F = F_1 + F_2$. We used that method to compute Newtonian configurations and compare them with semianalytical solutions. Figure 13 shows the error made with the same configuration as in Fig. 7 of [23] for a coordinate separation of 100 km. This calculation being Newtonian, the sources are compactly supported and the error seems to be evanescent, but we have to be cautious for the number of coefficients of the expansion is not maintained fixed. Extensive convergence properties have not been conducted but it seems that the splitting of the equation into two parts does not introduce any new Gibbs phenomenon. As for the single body problem, convergence of calculations with sources extending to infinity (i.e., in general relativity) has not been studied but we expect a Gibbs phenomenon to occur, because the sources contain almost every spherical harmonic.

To finish with the extension of this work let us mention the case of black holes. In that case the equations are not solved in all space but only on the domain exterior to the holes' horizons. This means that we have to remove the kernel from the computational domain. The regularity condition at the origin is then replaced by a boundary condition on the boundary of the innermost shell. We have been able to use that to impose a condition on the value of the solution (Dirichlet problem) or on its first radial derivative (Neumann problem). This extension has nothing to do with the compactified domain and we expect the convergence properties to be the same as those exhibited in the present work. We are currently applying this to compute realistic, physical binary black hole configurations.

7. CONCLUSION

We have presented a scalar Poisson equation solver based on a spectral method. It enables us to solve the Poisson equation for a source extending to infinity and going to zero at least like r^{-3}. Our multidomain approach enables us to deal with a source which is C^∞ in each domain. Nevertheless some Gibbs-like phenomena can appear due to the existence of particular solutions which contain logarithm functions in the external domain. Such functions are not well described in terms of Chebyshev polynomials, resulting in a Gibbs-like phenomenon. We exhibited the conditions for the appearance of such an effect and quantified it, leading to the conclusion that, for a source decaying as r^{-k} ($k \geq 3$), the error of the numerical solution is evanescent if the source does not contain any spherical harmonics with index $l \geq k-3$. Otherwise, the error decreases at least as $N^{-2(k-2)}$, N being the number of Chebyshev coefficients.

We used this scalar Poisson equation solver to solve the generalized vectorial Poisson equation given by Eq. (2) for a source going to zero at least like r^{-4}. Three different schemes have been discussed. We showed than the one proposed by Bowen and York [14] is not applicable to domains extending up to infinity, by means of our methods, because it gives rise to diverging auxiliary quantities. The scheme proposed by Oohara and Nakamura [15] is applicable as long as the source is continuous and has been successfully implemented. The last scheme, proposed by Oohara, Nakamura, and Shibata [16], is applicable even for discontinuous sources and has been successfully implemented too. The convergence properties of the two implemented schemes have been derived from the schemes of the scalar Poisson equation solver and checked by comparison between calculated and analytical solutions.

REFERENCES

1. E. Seidel and W.-M. Suen, Numerical relativity as a tool for computational astrophysics, *J. Comput. Appl. Math.* **109**, 493 (1999).
2. J. W. York, Kinematics and dynamics of general relativity, in *Sources of Gravitational Radiation*, edited by L. Smarr (Cambridge Univ. Press, Cambridge, UK, 1979).
3. Y. Choquet-Bruha, J. Isenberg, and J. W. York, Einstein constraints on asymptotically Euclidean manifolds, *Phys. Rev. D* **61**, 84,034 (2000).
4. L. Smarr and J. W. York, Radiation gauge in general relativity, *Phys. Rev. D* **17**, 1945 (1978).
5. J. W. York, Conformally invariant orthogonal decomposition of symmetric tensors on Riemannian manifolds and the initial-value problem of general relativity, *J. Math. Phys.* **14**, 456 (1973).
6. J. W. York, Covariant decomposition of symmetric tensors in the theory of gravitation. *Ann. Inst. Henri Poincaré*, t. **21**, 319 (1974).
7. J. W. York, Conformal “thin-sandwich” data for the initial-value problem of general relativity, *Phys. Rev. Lett.* **82**, 1350 (1999).
8. C. Canuto, M. Y. Hussaini, A. Quarteroni, and T. A. Zang, *Spectral Methods in Fluid Dynamics* (Springer-Verlag, Berlin, 1988).
9. D. Gottlieb and S. A. Orszag, *Numerical Analysis of Spectral Methods: Theory and Applications* (Society of Industrial and Applied Mathematics, Philadelphia, 1977).
10. S. Bonazzola, E. Gourgoulhon, and J.-A. Marck, Spectral methods in general relativistic astrophysics, *J. Comput. Appl. Math.* **109**, 433 (1999).
11. J. Frauendiener, Calculating initial data for the conformal Einstein equations by pseudospectral methods, *J. Comput. Appl. Math.* **109**, 475 (1999).
12. S. Bonazzola and J.-A. Marck, Three-dimensional gas dynamics in a sphere, *J. Comput. Phys.* **87**, 201 (1990).
13. S. Bonazzola, E. Gourgoulhon, and J.-A. Marck, Numerical approach for high precision 3-D relativistic star models, *Phys. Rev. D* **58**, 104,020 (1998).
14. J. M. Bowen and J. W. York, Time-symmetric initial data for black holes and black-hole collisions, *Phys. Rev. D* **21**, 2047 (1980).

15. K. Oohara and T. Nakamura, Coalescence of binary neutron stars, in *Relativistic Gravitation and Gravitational Radiation*, edited by J.-A. Marck and J.-P. Lasota (Cambridge Univ. Press, Cambridge, UK, 1997), p. 309.
16. K. Oohara, T. Nakamura, and M. Shibata, A way to 3D numerical relativity, *Prog. Theor. Phys. Suppl.* **128**, 183 (1987).
17. R. Dautray and J.-L. Lions, *Analyse Mathématique et Calcul Numérique Pour les Sciences et les Techniques*, (Eds Masson, 1987), t. **2**.
18. L. Tuckerman, Transformations of matrices into banded form, *J. Comput. Phys.* **84**, 360 (1989).
19. Linear Algebra PACKage, available at http://www.netlib.org/lapack/.
20. E. Gourgoulhon, P. Haensel, R. Livine, E. Paluch, S. Bonazzola, and J.-A. Marck, Fast rotation of strange stars, *Astron. Astrophys.* **349**, 851 (1999).
21. N. Ó Murchadha, Boundary conditions for the momentum constraint, in *Approaches to Numerical Relativity*, edited by R. d'Inverno (Cambridge Univ. Press, Cambridge, UK, 1992).
22. S. Bonazzola, E. Gourgoulhon, and J.-A. Marck, Numerical models of irrotational binary neutron stars in general relativity, *Phys. Rev. Lett.* **82**, 892 (1999).
23. E. Gourgoulhon, P. Grandclément, K. Taniguchi, J.-A. Marck, and S. Bonazzola, Quasiequilibrium sequences of synchronized and irrotational binary neuron stars in general relativity. I. Methods and tests, *Phys. Rev. D* **63**, 064,029 (2001).